powders

MDPI

Article

Reuse of Smoulder in Laser Powder-Bed Fusion of AlSi10Mg—Powder Characterization and Sample Analysis

Oliver Maurer [1,2,*], Heiko Jacob [3] and Dirk Bähre [1,2]

[1] Institute of Production Engineering, Saarland University, Campus A4.2, 66123 Saarbruecken, Germany
[2] Centre for Mechatronics and Automation Technology ZeMA, Eschberger Weg 46, 66121 Saarbruecken, Germany
[3] Fraunhofer Institute for Nondestructive Testing IZFP, Campus E3.1, 66123 Saarbruecken, Germany
* Correspondence: oliver.maurer@uni-saarland.de

Abstract: Metal additive manufacturing technologies, such as Laser Powder-Bed Fusion, often rate as sustainable due to their high material efficiency. However, there are several drawbacks that reduce the overall sustainability and offer potential for improvement. One such drawback is waste emerging from the process. These smoulder particles form when the laser hits the powder-bed surface, are blown away from the part by the shielding gas stream and accumulate on the edge of the build chamber. Usually, smoulder does not contribute to the circular reuse of powder that was part of the powder-bed but was not integrated into a part. Instead, it marks an end-of-life state of powder. Significant amounts of smoulder accumulate depending on the irradiated area or the build volume in one job, respectively. This results in the waste of powder that was produced with low energy efficiency. This study investigates the question of whether smoulder can transform from waste to resource via common powder characterization methods and first build jobs using processed smoulder. The investigation of process-relevant powder properties like apparent density and flowability showed no significant difference between virgin powder and smoulder. Sample characterization indicated that neither porosity, surface quality nor mechanical properties deteriorate when samples contain about 50% smoulder. This allows for the reuse of smoulder in terms of powder characterization and part quality.

Keywords: L-PBF; powder characterization; smoulder recycling; material efficiency; AlSi10Mg

Citation: Maurer, O.; Jacob, H.; Bähre, D. Reuse of Smoulder in Laser Powder-Bed Fusion of AlSi10Mg—Powder Characterization and Sample Analysis. *Powders* **2024**, *3*, 154–167. https://doi.org/10.3390/powders3020010

Academic Editor: Paul F. Luckham

Received: 18 December 2023
Revised: 13 March 2024
Accepted: 25 March 2024
Published: 27 March 2024

1. Introduction and State of the Art

Additive manufacturing (AM) has revolutionized science and various industries due to its high degree of geometrical freedom in design [1]. Highly individual products of small batch sizes down to one appeal to biomedical, aerospace and automotive or more general lightweight applications [2]. AM processes gain flexibility by building parts directly from a sliced CAD-model in a layer-by-layer fashion without the need for any tools [3,4]. However, these technologies are subject to geometrical restrictions and require design for additive manufacturing (DfAM) guidelines to be followed [4]. Laser Powder-Bed Fusion (L-PBF) is a popular technology used to manufacture metallic parts from a powder. In L-PBF, a laser completely melts powder particles along its path, fusing the raw material [5]. Generally, all weldable materials fit the L-PBF process [4], but part properties strongly depend on the material used, powder properties and process parameters [6–8]. Due to the importance of heat flow during the process represented by energy density definitions [9], AM is not suitable for producing large bulk parts of simple geometry [10]. This technology produces near net-shape parts that require post-processing to meet high-quality specifications [2]. Usually, significant amounts of porosity, rough surfaces, anisotropic microstructures and poor geometrical accuracy mark L-PBF parts in the as-built state [11–14].

As sustainability of products and manufacturing systems becomes increasingly important, the literature has already addressed the performance of L-PBF. The four dimensions

of sustainability focus on ecological, economic, societal and technical aspects [15,16]. Hapuwatte et al. [17] found that additively manufactured parts can be more sustainable from an ecological perspective if their design includes high degrees of geometric complexity and lightweight optimization. Although a part may be highly optimized with respect to DfAM, Kellens et al. [18] have identified potential sustainability improvements by reducing energy consumption of L-PBF machines. Another issue is waste of powder material due to filter residues, aerosol emission and smoulder formation. Based on this finding, Kellens et al. suggest that reducing material waste would create a sustainable impact. Dopler et al. [19] support this hypothesis by calculating an energetic degree of efficiency for different gas atomization powder production setups, which is less than 1% in all scenarios studied for a general powder material. To achieve sustainability in L-PBF, powder reuse should be maximized to as close to 100% as possible.

Smoulder occurs as an unavoidable phenomenon during the process and affects the interaction between the laser beam and powder-bed in L-PBF [20] and other metal AM technologies [21]. Smoulder particles differ from virgin powder in color [20] and size, reaching from nanoscale to coarser than virgin powder [22,23]. They tend to congregate on the surface they formed above. To prevent part contamination, a fast stream of inert gas flows across the powder bed and carries smoulder particles away from the powder bed, causing them to congregate on the side of the build chamber instead [24].

Only a few studies have investigated the characteristics of smoulder particles, which are typically disposed after the completion of a build job. In the case of stainless steel, chemical composition and crystal structure appear to remain unchanged throughout the transformation from virgin powder to smoulder [20]. For Ti6Al4V, one study detected no change in composition [25] and one study did [26]. However, smoulder particles form a thicker oxide layer than virgin powder counterparts, but this does not affect the bulk properties of particles [27]. The thickness of oxide layers on IN718 smoulder particles decreases with lower oxygen content during the build job [25]. Murray et al. [28] found an influence of smoulder content on single-track volumes which is rather negligible if it is blended with virgin powder [24]. The literature rather covers the reuse of powder that was part of a powder-bed several times but was not included in fabricated parts due to the influence of powder properties such as particle morphology, particle size distribution or powder flowability. These characteristics influence the overall processability in L-PBF as well as part properties [29]. According to Weiss et al. [30], the concentrations of Al, Si, Mg and H remained almost constant in powders with up to 10 use cycles. Throughout the use cycles, the oxygen concentration increased. Del Re et al. [31] reported a decrease in tensile properties including yield strength, ultimate tensile strength, elongation at break and high cycle fatigue strength when the AlSi10Mg powder was reused up to 8 times. Moghimian et al. [32] and Smolina et al. [33] reached similar conclusions of comparable tensile properties of samples from virgin and reused powder of AlSi10Mg and AlSi7Mg0.6. If L-PBF process parameters and powder quality control or powder preparation are set properly, reused powder can serve as a feedstock material to high-quality parts [33,34].

In summary, the current state of research covers the formation and basic properties of smoulder particles but does not investigate their impact on part properties when blended in virgin powder to produce parts. Despite the enhanced sphericity of these particles [23], there is no information available on their processability. This study aims to address this issue by conducting process-relevant powder characterization of AlSi10Mg-smoulder and producing parts including smoulder, followed by quality assessment. If smoulder can be reused as feedstock material without comprising processability and part quality, the material efficiency of L-PBF would increase and less waste would be generated.

2. Materials and Methods

2.1. L-PBF Machine and Virgin Powder

This study examines smoulder formation during build jobs of a SLM125 L-PBF machine by Nikon SLM Solutions Group AG (Lübeck, Germany). The machine has a cube-

shaped build volume of 125 mm edge length and AlSi10Mg from the same provider serves as the virgin powder with a nominal size distribution from 20 µm up to 63 µm. Table 1 summarizes its chemical composition as per its material data sheet. Smoulder particles are collected from several build jobs in order to gain enough to fabricate parts. Therefore, the collected smoulder particles were stored for several weeks before analysis and part fabrication. During this time, the collected particles were kept in closed containers inside a safety storage cabinet.

Table 1. Chemical composition of virgin AlSi10Mg-powder used in this study [35].

Elements	Al	Si	Fe	Mg	Mn	Ti	Zn	Others Each
Wt.%	Bal.	9–11	0.55	0.45	0.45	0.15	0.10	0.05

2.2. Powder Characterization Techniques

Morphology. Aspect ratios act as main characteristics of particle morphology. Several samples with a total basic population of 5746 smoulder particles and 3871 virgin powder particles were analyzed with a VHX7000 digital microscope (Keyence Corp., Osaka, Japan), which can analyze particle sizes automatically. The aspect ratio and its distribution were then calculated as the quotient of the minimum divided by maximum particle diameter. The closer values are to one, the more spherical the particle is.

Phase analysis. Samples of virgin powder and smoulder were characterized in powder X-ray diffraction (XRD) with CuK_{α}-radiation. The purpose of this analysis was to determine the powders' crystal structures and identify non-metallic phases present. Therefore, a Bruker D8-A25-Advance (Bruker Corp., Billerica, MA, USA) was used. A Rietveld analysis helped to assign Miller indices to peaks in the XRD pattern and helped to find crystals of common oxides, which the alloying elements tend to form. Standard data for comparison with measurements come from the Crystallography Open Database and Pearson's Crystal Data.

Powder size distribution. Samples of virgin powder and smoulder were analyzed with a laser granulometer HELOS H2482 (Sympatec GmbH, Clausthal-Zellerfeld, Germany) and its analyzing software WINDOX 5. The measurement results included particle size distributions and cumulative curves of relative frequencies, which allow for determination of characteristic diameters d_{10}, d_{50} and d_{90}. This kind of diagram can be used to determine the loss of powder and smoulder during sieving. The percentage of particles which can pass the sieving process equals a theoretical recycling rate.

Powder flowability. A standardized Hall funnel in accordance with EN ISO 4490 [36] was used to assess the first characteristics of powder flow behavior. It does not represent the in-process coating behavior, but gives sufficient quantifications [37]. The funnel was filled with 50 g of powder, resulting in a mean flow rate $\frac{dm}{dt}$ (mass flow per passed time), which was measured by timing how long it takes to empty the funnel completely. The moisture content of the investigated powder sample acts as crucial boundary condition that affects flowability. Therefore, the dew-point sensor HYTE-LOG 4800 Bd (Hygrosens Instruments, Löffingen, Germany) was used to measure the moisture content and provide information on comparability between measurements.

Apparent density. A standardized container with a volume of (25 ± 0.03) cm^3 in accordance to EN ISO 3923 [38] was filled entirely. Powder particles fell out of a Hall funnel mounted 25 mm above the container to achieve a reproducible particle packing. Afterwards, the container was weighed on an AT200 (Mettler Toledo Inc., Columbus, OH, USA) precision scale with a tolerance of 0.01 g. The apparent density is then given by the measured sample mass divided by the container's volume. Three repetitions assure reliable measurements.

2.3. Sample Fabrication and Quality Assessment

L-PBF build jobs. Smoulder for part fabrication was collected from several build jobs to produce easy to inspect samples with a sufficient smoulder content. Afterwards, smoulder becomes part of the usual Argon-shielded sieving routine with a mesh width of 75 µm together with virgin powder. Therefore, it is difficult to determine the exact proportions of smoulder in the blend with virgin powder, but it is likely that the blend consists of 50% virgin powder and 50% smoulder.

A simple plate-like geometry was chosen to assess the impact of smoulder in parts. The samples measure 30 mm by 3 mm and 100 mm in height (see Figure 1). The smoulder region was about 60 mm in height, while the rest of the sample consisted of virgin powder, which laid above the smoulder region in the powder feedstock. Three cylindrical holes allowed us to assess smoulder congregation at geometrical features. Table 2 presents the most important process parameters, which have been demonstrated to yield satisfactory quality for thick-walled parts [11]. Furthermore, the substrate was heated to 423 K (150 °C) to reduce residual stress formation. The build job of smoulder-containing parts lasted 22 h. The hatch scan strategy involves dividing each irradiated area into its contour and its center, where the laser scans the area in patches with a maximum track length of 10 mm.

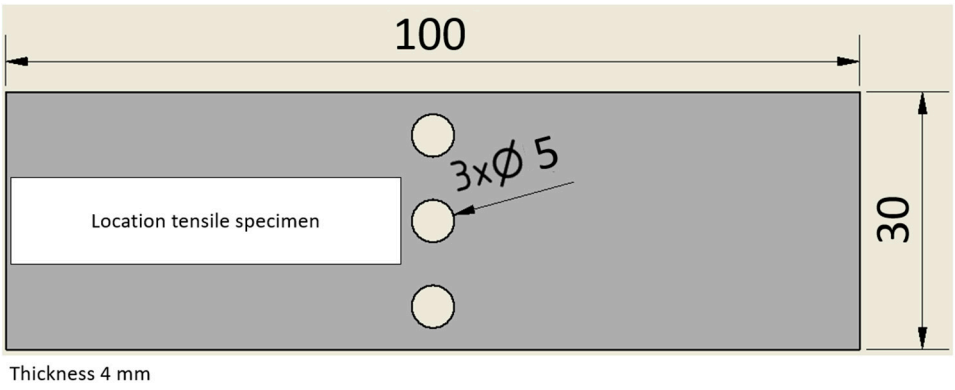

Figure 1. Sample geometry fabricated with a smoulder content of 50%; all measures in mm.

Table 2. L-PBF process parameters used to manufacture smoulder-containing samples.

Parameter	Powder Layer Thickness	Laser Power	Scan Speed	Hatch Distance	Substrate Heating	Scan Strategy	Shielding Gas
Value	30 µm	250 W	1650 $\frac{mm}{s}$	0.13 mm	423 K	Hatch	Argon

All the samples remained in their as-built state after fabrication. However, the surface of each plate facing towards the substrate was post-processed by sawing the samples off the substrate. First, visual inspection and metallographic preparation on SiC-sandpaper (320–1200 graining) and textile polishing cloths (6 µm–1 µm diamond suspension) without etching were carried out to find obvious defects on surfaces and non-metallic inclusions. Polished samples were examined using the digital microscope VHX-7000 (Keyence Corp., Osaka, Japan).

Surface quality. Stylus profilometry with a Perthometer PGK120 (Mahr GmbH, Göttingen, Germany) was used to assess central and peak core roughness R_k and R_{pk} according to EN ISO 13565 [39] and divide a profile of L-PBF samples into its center driven by laser scan paths, powder layers or parameter-related phenomena like balling and a top region driven by particle adhesion. Values were extracted from a profile using an Abbott–Firestone curve, a cumulative frequency plot of heights $z(x)$ in a roughness profile. In this study, five scan lengths of 2.5 mm as well as 1.25 mm scan lengths for transient stylus oscillations at the beginning and the end of each track lead to a total scan length of 15 mm per measurement. The related critical wavelength of the waviness filter equals 2.5 mm.

Relative density. Relative density was measured as a counterpart to porosity using the precision balance AT200 (Mettler Toledo Inc., Columbus, OH, USA) equipped with a setup for Archimedean density measurements. Each sample was weighed three times in air and three times in water of a known temperature. The water container sat on the frame of the balance and did not affect weighing results. Measurements in water were conducted in a mesh basket suspended from a boom, which was directly connected to the measuring unit of the balance. Depending on the water's density $\rho_w(T)$, the alloy's theoretical density $\rho_{th} = 2.67\ \mathrm{g/cm^3}$ [35] and the sample masses in air m_a and in water m_w, the relative density follows as:

$$\rho_r = \frac{1}{\rho_{th}} \frac{m_a\ \rho_w(T)}{m_a - m_w} \tag{1}$$

Tensile properties. Plate-shaped dog-bone tensile specimens with a cross-section of 9 $\mathrm{mm^2}$ and a gauge length of 20.2 mm were machined by milling all surfaces from the plate-shaped L-PBF samples. Destructive testing was performed with an ElectroPuls E10000 (Ltd. Instron, Pfungstand, Germany) with a displacement rate of 0.02 mm/s. Matlab R2023b software (Mathworks Inc., Natick, MA, USA) was used for data curation and calculation of elongation at failure, ultimate tensile strength and yield strength. The tensile properties of five smoulder-containing samples were tested.

3. Results and Discussion

3.1. Powder Characterization of Smoulder versus Virgin Powder

Throughout sieving, smoulder particles mix with virgin powder and characterization loses accuracy. This is why basic powder properties as given in Table 3 are measured in a not-sieved state.

Table 3. Powder characteristics regarding flowability, apparent density and particle sizes of smoulder and virgin powder.

Powder Property	Smoulder	Virgin Powder	State
Relative moisture content/%	36.25	8.87	Not sieved
Flowability/g/s (EN ISO 4490)	0.81 ± 0.02	0.61 ± 0.01	
Apparent density ρ_A/g/cm^3 (EN ISO 3923)	1.92 ± 0.00	1.29 ± 0.01	
Maximum diameter of 10% of particles d_{10}/µm	36.33	26.28	
Maximum diameter of 50% of particles d_{50}/µm	68.24	43.29	
Maximum diameter of 90% of particles d_{90}/µm	139.90	68.59	
Theoretical recycling rate/% ($d \leq 75$ µm)	57%	95%	

The comparably high moisture content of smoulder particles is probably due to storage for several weeks without treatment and would probably decrease during sieving, so in the process it provides a sufficient moisture content. Sieving decreases the relative moisture content because the process runs under an atmosphere of dry argon. An ultrasonic transducer shakes the whole capsuled sieve and makes particles fall one by one through the mesh into a container. During this forced motion, moisture can be separated from the powder. However, this happens to a lower extent than with a drying cabinet. The flowability of smoulder rates as sufficient because its value is still larger than that of virgin powder, despite the higher moisture content leading to a decrease in powder flow. However, the flowability and apparent density exceed those of virgin powder probably due to larger particles (see Table 3 and Figure 3c). This effect will decrease during sieving, but it may result in superior spreading behavior and a denser powder-bed in the L-PBF process. Characteristic particle diameters show that smoulder is much coarser than virgin powder. Sieving with a mesh size of 75 µm removes coarser fractions anyway, which results in an availability of about 57% of smoulder particles and 95% of virgin powder for a build job and which basically gives a theoretical recycling rate of different powder types. However, this value does not account for losses during powder removal from the build chamber or support structures and parts.

In microscopic analysis, particles lay as dense as shown in Figure 2a,b. Closer packing could lead to misinterpretations in automatic analysis as particle accumulations would be treated as one large particle. Five images per powder type, such as these, provide the aforementioned amounts of analyzed particles. Zoom sections display typical particle morphologies, including agglomerates and satellites. Especially in the smoulder images, there are elongated particles and satellites, while agglomerates can be observed for both powder types.

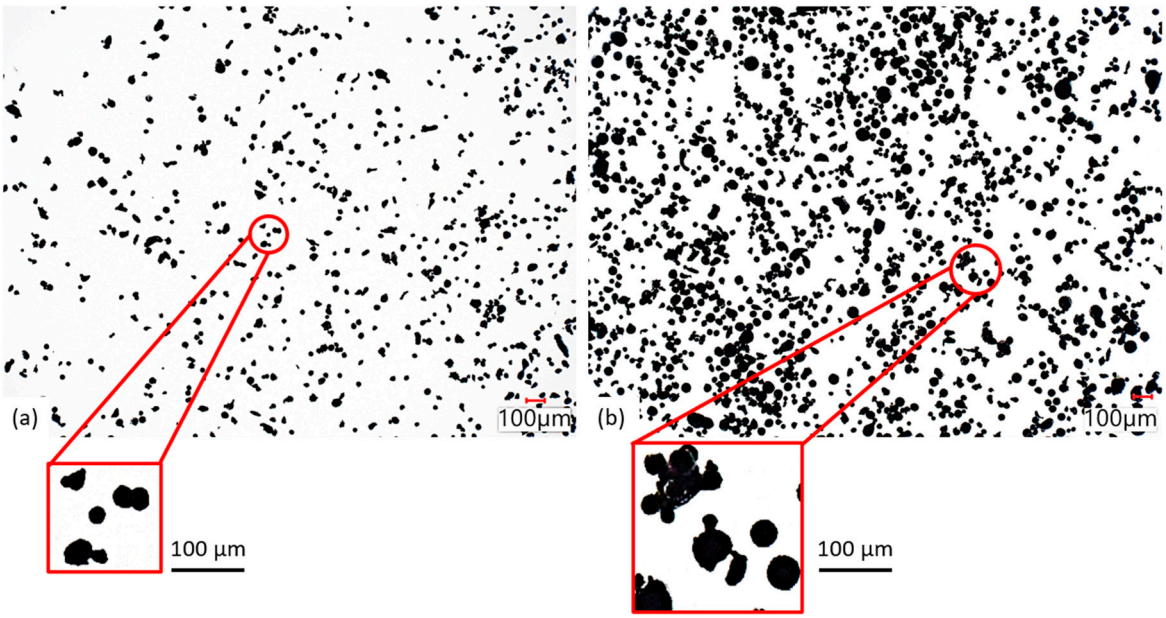

Figure 2. Examples of transmitted light microscopy of powder particles to calculate morphology data: (**a**) virgin powder and (**b**) smoulder.

The distribution of aspect ratios, as shown in Figure 3a, reveals that most particles have a rather spherical shape. Although the maximum is at about 0.8, indicating that most particles are slightly deformed or have satellites attached to their surfaces, the particle morphology distributions do not differ in shape but in height due to different sample sizes. The cube-shaped build volume V_{build} with an edge length of 125 mm contains a tremendous number of particles. If all particles had the same diameter of d_{50} and were packed in the apparent density ρ_A, it follows for the maximum amount of particles in the build volume n_{max} with the help of the theoretical density of AlSi10Mg $\rho_{th} = 2.67\ \frac{g}{cm^3}$ [35]:

$$n_{max} = \frac{\rho_A}{\rho_{th}} * \frac{6\ V_{build}}{\pi d_{50}^3} \approx 2.2 * 10^{10} \tag{2}$$

Consequently, the sample sizes of virgin powder and smoulder equal portions of $1.76 * 10^{-7}$ and $2.61 * 10^{-7}$ of a completely filled build volume. These samples provide a first impression on distributions but do not represent amounts of powder in a L-PBF process. As a consequence, real distributions of real build volumes may vary.

Phase composition measured via powder-XRD as depicted in Figure 3b appears very similar when comparing smoulder to virgin particles. After conducting a Rietveld analysis on both patterns all peaks were assigned to Al, Si, $Al_{0.6}Mg_{0.4}$ and $Al_{0.68}Mg_{0.32}$ in fcc crystals. Indexed Rietveld data of the virgin powder sample are given in Appendix A. These patterns match those of Lam et al. [40]. Their XRD patterns assign identical Miller indices to peaks of the main phases Al and Si at the same angles as depicted in Figure 3b. XRD did not detect any oxide-related crystal structures in either the virgin powder or the smoulder sample, so smoulder does not contain large amounts of oxide phases. This does not prove the absence of oxygen concentration on the surface of smoulder particles or the absence of oxygen

solution inside the particle. It is important to note that there are several ways for oxygen to accumulate in L-PBF parts, even if they are fabricated from virgin powder, and this study did not investigate the oxygen pollution of powder particles. However, Lam et al. [40] found an oxygen content of 1.87 wt.% in as-built samples, which were fabricated from virgin powder. It remains to be investigated whether possibly larger oxygen pollutions of smoulder particles cause higher oxygen concentrations in as-built parts due to the fact that there is excess oxygen in build jobs anyway.

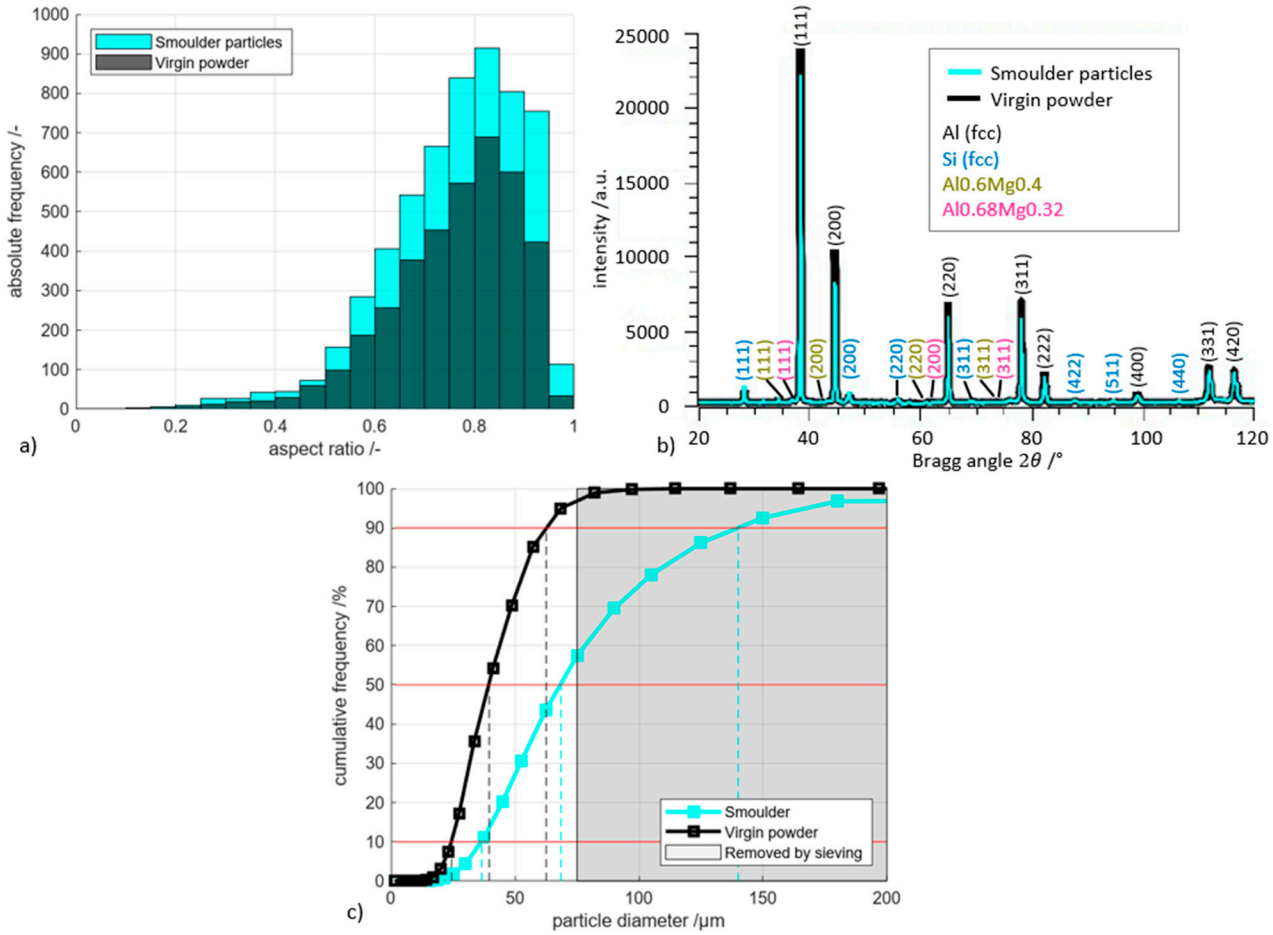

Figure 3. (**a**) Particle morphology distribution, (**b**) indexed XRD pattern and (**c**) particle size distribution of smoulder compared to virgin powder.

From a powder characterization perspective, smoulder of the AlSi10Mg alloy can be reused after sieving in L-PBF due to its high similarity to virgin powder in process-relevant properties. During the sieving process, larger amounts of particles are sorted out by their size if compared to virgin powder, which can still contribute to higher material efficiency without disturbing layer spreading behavior.

3.2. Part Quality of Smoulder-Containing Samples

Smoulder and virgin powder are sieved before serving as a feedstock material in the L-PBF process. Smoulder-containing regions of all samples show a different coloration than the regions fabricated from virgin powder. As depicted in Figure 4, coloration of powder particles matches surface coloration of a sample (a–c). After exemplarily sandblasting one sample (d), surfaces of smoulder-containing and virgin regions appeared almost identical, suggesting that effects localize in a very thin zone at the surface. Geometrical features like cylindrical holes do not seem to influence surface coloration, as there is no accumulation of smoulder colors at their contours. This leads to the conclusion that smoulder usage in

a build job does not result in visible gradients of properties and does not affect quality. Different parameter regimes inside a scan pattern may explain near surface color changes. The parameter set used in this study irradiates the core of each layer first with the hatch parameter and, after that, the contour with adjusted parameters. Crystallization kinetics may then push color changing particles inside the melt pool to the surface of the part.

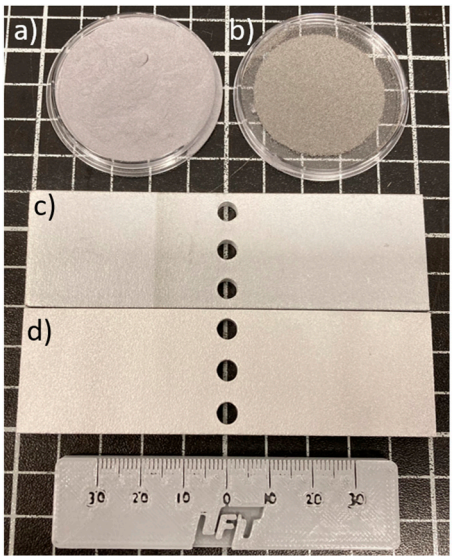

Figure 4. (**a**) Virgin powder, (**b**) smoulder, (**c**) as-built sample including virgin and smoulder-containing regions and (**d**) sandblasted sample, scale in mm.

The relative density of smoulder-containing samples is similar to the relative density of samples from virgin powder, with values of $(99.7 \pm 0.2)\%$ and $(99.9 \pm 0.1)\%$, respectively, due to overlapping scatter intervals. Smoulder seems to slightly increase porosity and its scatter. However, if there was a porosity formation mechanism triggered by smoulder usage, differences would have been more evident. Metallographic cross sections confirm the values obtained from Archimedean density measurement, even if the two-dimensional information of one cross section does not represent a three-dimensional distribution of pores properly. As depicted in Figure 5, stitched micrographs reveal similar amounts of pores but there are no non-metallic inclusions or other defects visible that could affect the degree of purity. Metallographic analysis found no reason to avoid using smoulder as a powder material, supporting the assumption that impurities are pushed towards the surface and the center of the part remains unchanged.

The roughness measurements on the surfaces of smoulder-containing and virgin samples resulting in Table 4 do not differ from each other, regardless of the measuring direction. Slightly differing mean values of core roughness values R_k and R_{pk} of the smoulder region are covered by scatter intervals of surfaces fabricated from virgin powder. Additionally, peak core roughness R_{pk} reveals that there is practically no difference in the degree to which powder particles adhere to a surface.

Table 4. Core roughness values of smoulder-containing and virgin powder regions; mean values of five measurements.

Roughness Type	Smoulder-Containing Region	Region from Virgin Powder
Core roughness R_k/µm	Building direction: 12.5 ± 1.1 Interlayer roughness: 11.5 ± 3.0	Building direction: 13.0 ± 1.3 Interlayer roughness: 12.0 ± 1.9
Peak core roughness R_{pk}/µm	Building direction: 10.4 ± 2.6 Interlayer roughness: 10.9 ± 3.6	Building direction: 9.0 ± 4.5 Interlayer roughness: 10.1 ± 2.6

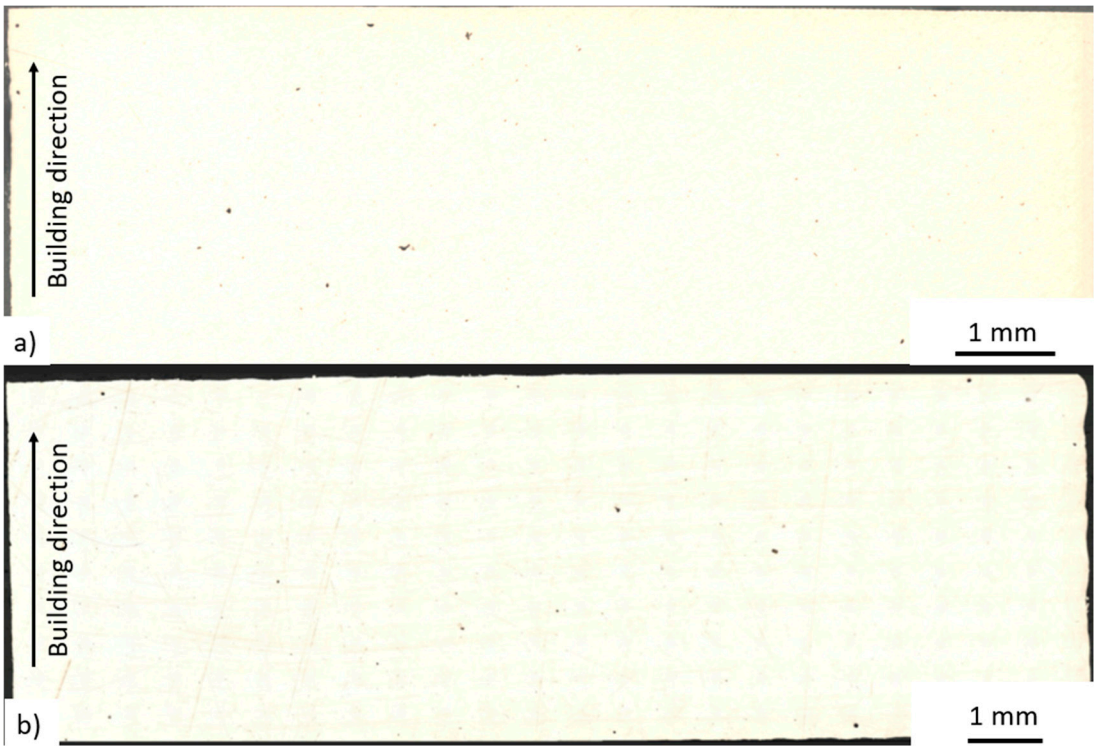

Figure 5. Metallographic cross sections fabricated by L-PBF (**a**) from virgin powder and (**b**) smoulder-containing samples.

Tensile tests of smoulder-containing samples allow to compare mechanical key properties to standard values given by the material data sheet of AlSi10Mg [35]. Figure 6 shows only minor variations in the linear-elastic regions representing stiffness. The curves of samples 3 and 4 superpose in the diagram, making only four curves clearly visible. All five samples failed at a similar elongation as depicted in Figure 6 and noted in Table 5. These values are nearly identical to those of [41] for a similar parameter set. The ultimate tensile strength (UTS) varies more widely, with a range twice as large as that of the material data sheet. Besides this, UTS exceeds the value from the data sheet by about 64 MPa on average, which compensates for the larger scatter. Additionally, UTS also exceeds data from the literature. The parameter set used by Sert et al. [42] differs more from the one used in this study than the one in [41]. This study's values differ from those found in data sheets or the literature, primarily because the tensile specimens were cut solely from hatch parts of larger L-PBF samples. Parameter sets with distinct hatch and contour parameter regimes apply locally different laser power and scan speed, which may affect cracking behavior in a tensile test and ultimately decrease the UTS. The yield strength and its scatter also exceed the comparative values. This indicated that smoulder-containing samples require higher stress levels to deform plastically, which may occur if dislocations movement is inhibited by factors such as precipitation hardening. Further investigations are necessary to determine the distribution of oxygen within smoulder-containing parts. Lam et al. [40] have already reported the oxygen distribution for samples fabricated from virgin powder. If the assumption was true, the oxygen distribution in smoulder-containing samples must differ from that. However, if data sheet values form the foundation for part design calculations, smoulder-containing parts can meet this requirement. So, from this perspective, there is no reason against using smoulder as a powder material.

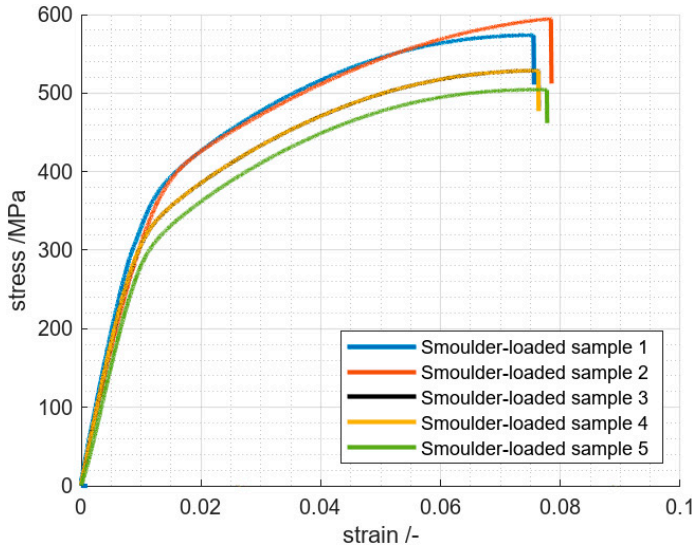

Figure 6. Engineering stress–strain curves of smoulder-containing samples fabricated by L-PBF.

Table 5. Tensile properties of smoulder-containing L-PBF-AlSi10Mg samples in comparison to samples fabricated from virgin powder; mean values of five samples.

Tensile Property	Smoulder-Containing Samples	Material Data Sheet from Powder Provider [35]	Ghio and Cerri [41] at Similar Process Parameters	Sert et al. [42]
Elongation at failure/-	0.077 ± 0.001	0.05 ± 0.02	0.076 ± 0.01	0.052 ± 0.048
Ultimate tensile strength/MPa	546.3 ± 36.9	482 ± 15	463 ± 3	352.1 ± 8.9
Yield strength at 0.2% plastic strain/MPa	310.6 ± 16.2	248 ± 5	237 ± 4	226.1 ± 8.1

4. Conclusions and Future Research

This study presents a profile of smoulder particles formed in an argon-shielded L-PBF process with AlSi10Mg powder and assesses key part quality features. In summary, processability of smoulder to serve as a powder raw material is subject to the investigations of this contribution leading to the following main findings:

- The powder properties of smoulder are very similar to virgin powder. Due to larger particles, flowability and apparent density exceed values for virgin powder, this effect will decrease after sieving;
- Since all types of powder are sieved before serving in a build job, a maximum of 57% of smoulder particles can be reused. Virgin powder reaches a value of 95% according to the comparison of particle size distribution and sieving mesh size;
- The phase compositions of both powder types coincide and did not reveal the presence of oxides or other non-metallic phases that could disturb the degree of purity in a manufactured part. This does not mean a negligible oxygen content in the feedstock. As Moghimian et al. [32] pointed out, chemisorption and physical adsorption of oxygen on powder particles may introduce undesirable oxygen into the L-PBF process without being detected as oxide crystals in XRD;
- Macroscopic changes in coloration are limited to the surface only, which can be removed with sand blasting due to its thin-ness;
- The microscopic properties of smoulder-containing samples are very similar to those fabricated from virgin powder. Degree of purity analysis revealed similar porosity for both sample types which is supported by Archimedean density measurements;
- The presence of smoulder has no impact on surface core roughness or particle adhesion from the surrounding powder-bed;

- Tensile tests show a higher elongation at failure, ultimate tensile strength and yield strength than given in the material data sheet from the powder provider;
- All results point towards using smoulder as feedstock material at least once. It still remains unclear whether multiple reuses of smoulder lead to excessive oxygen contents in parts. Even in the first run the oxygen distribution may affect tensile properties and requires further investigations in future studies.

All in all, this study found no evidence to keep wasting smoulder of L-PBF-AlSi10Mg. Neither process-relevant powder characteristics, nor key part properties like degree of purity, surface roughness, porosity and tensile properties decrease in quality suffer from negative effects of smoulder. Only scatter intervals may grow, but do not compromise process reliability. The real impact of smoulder content on scatter intervals should be a subject to a study as in [11], so adjusted tolerance bands for smoulder-containing parts can be compared to those for standard parts. This may help to define a threshold oxygen content of powder and part.

Based on these findings, smoulder should rather serve as a raw powder material and thereby advance material efficiency of the L-PBF process. Further characterizations of smoulder-containing parts shall clarify whether this hypothesis is correct and provide sufficient statistical confidence. The purity of structures, where almost every part of the volume lies close to a surface, like lattice structures must be investigated if impurities tend to congregate at the surface.

Author Contributions: Conceptualization, O.M.; methodology, O.M. and H.J.; software, H.J.; validation, O.M.; formal analysis, O.M.; investigation, O.M. and H.J.; resources, O.M.; data curation, H.J.; writing—original draft preparation, O.M.; writing—review and editing, D.B.; visualization, H.J.; supervision, D.B.; project administration, D.B.; funding acquisition, D.B. All authors have read and agreed to the published version of the manuscript.

Funding: This research received funding from Deutsche Forschungsgemeinschaft (DFG) in the State Major Instrumentation program with the reference INST 256/503-1 FUGG.

Institutional Review Board Statement: Not applicable.

Informed Consent Statement: Not applicable.

Data Availability Statement: The raw data supporting the conclusions of this article will be made available by the authors on request.

Acknowledgments: The L-PBF machine used to produce the specimens in this contribution was generously funded by Deutsche Forschungsgemeinschaft (DFG) in the State Major Instrumentation program with the reference INST 256/503-1 FUGG.

Conflicts of Interest: The authors declare no conflict of interest.

Appendix A

The XRD patterns of Figure 3b include phases $Al_{0.6}Mg_{0.4}$ and $Al_{0.68}Mg_{0.32}$. Related peaks are shown more clearly in the standardized Rietveld data of Figure A1. Both phases are not part of the crystallographic data bases used, but $Al_{0.63}Mg_{0.37}$ is. Indexed Al-Mg phases describe corrected stoichiometries with respect to Vegard´s law. Since Mg crystallizes in a hexagonal structure [43], calculations of a representative lattice constant require a transformation to a fcc proxy phase. It is with values for $Al_{0.63}Mg_{0.37}$ from data bases:

$$a_{proxy} = \frac{a_{Al0.63Mg0.37} - x_{Al}a_{Al}}{1 - x_{Al}} = \frac{4.213\ \text{Å} - 0.63 * 4.050\text{Å}}{0.37} = 4.491\ \text{Å} \quad \text{(A1)}$$

All a_i represent lattice constants of their respective phases according to the data base and all x_i represent mole fractions of phases given by their stoichiometry. Additionally, in Al-Mg phases it is $x_{Al} + x_{Mg} = 1$. Finally, the proportion of aluminum in the solid solution (index 'mix') can be determined in terms of the mole fraction. Consequently, the correct

stoichiometric composition of the solid solution can be determined in the form Al_xMg_{1-x}. It is:

$$x_{Al} = \frac{a_{mix} - a_{proxy}}{a_{Al} - a_{proxy}} \quad \text{(A2)}$$

Data bases provide two different lattice constants a_{mix} for the solid solution of Mg in Al and therefore corrected stoichiometries are $Al_{0.6}Mg_{0.4}$ and $Al_{0.68}Mg_{0.32}$.

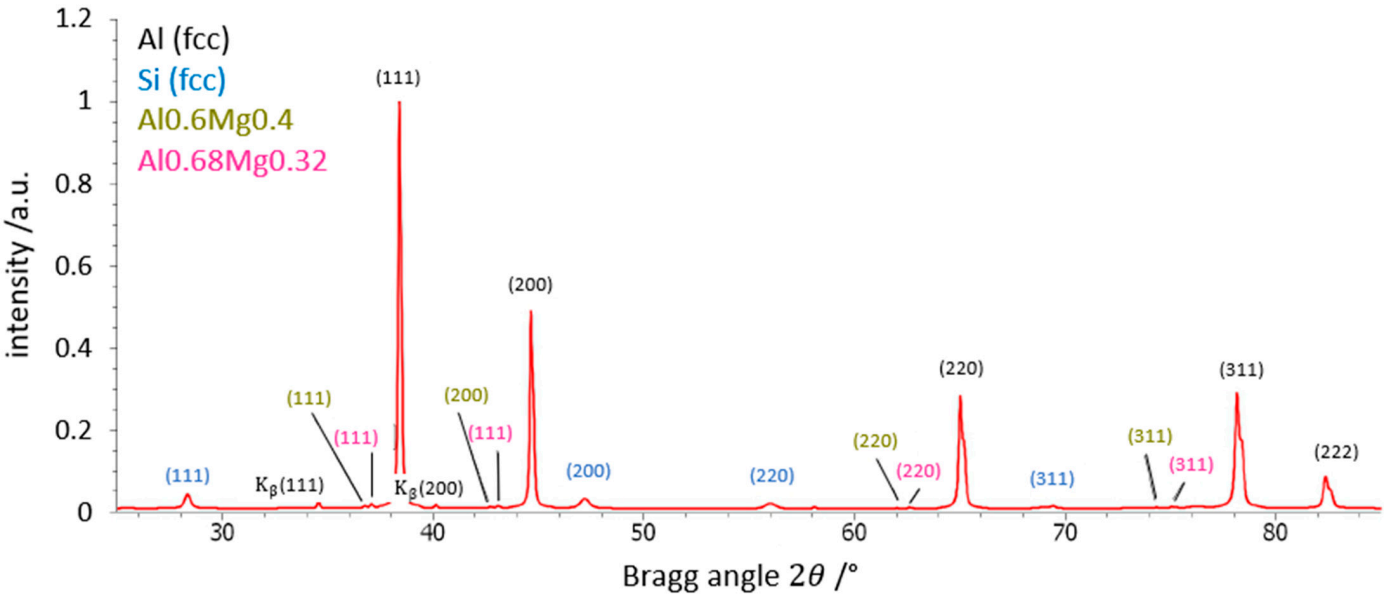

Figure A1. Standardized Rietveld data of virgin powder XRD as indexed by the software.

References and Note

1. Sing, S.L.; Yeong, W.Y. Laser powder bed fusion for metal additive manufacturing: Perspectives on recent developments. *Virtual Phys. Prototyp.* **2020**, *15*, 359–370. [CrossRef]
2. Yap, C.Y.; Chua, C.K.; Dong, Z.L.; Liu, Z.H.; Zhang, D.Q.; Loh, L.E.; Sing, S.L. Review of selective laser melting: Materials and applications. *Appl. Phys. Rev.* **2015**, *2*, 041101. [CrossRef]
3. Godec, D.; Gonzalez-Gutierrez, J.; Nordin, A.; Pei, E.; Ureña Alcázar, J. (Eds.) *A Guide to Additive Manufacturing*; Springer Tracts in Additive Manufacturing; Springer International Publishing: Cham, Switzerland, 2022; ISBN 978-3-031-05862-2. [CrossRef]
4. Gibson, I.; Rosen, D.; Stucker, B.; Khorasani, M. *Additive Manufacturing Technologies*; Springer International Publishing: Cham, Switzerland, 2021; ISBN 978-3-030-56126-0. [CrossRef]
5. Sun, S.; Brandt, M.; Easton, M. Powder bed fusion processes. In *Laser Additive Manufacturing*; Elsevier: Amsterdam, The Netherlands, 2017; pp. 55–77. ISBN 978-0-08-100433-3. [CrossRef]
6. Frazier, W.E. Metal Additive Manufacturing: A Review. *J. Mater. Eng. Perform.* **2014**, *23*, 1917–1928. [CrossRef]
7. Zhang, J.; Song, B.; Wei, Q.; Bourell, D.; Shi, Y. A review of selective laser melting of aluminum alloys: Processing, microstructure, property and developing trends. *J. Mater. Sci. Technol.* **2019**, *35*, 270–284. [CrossRef]
8. Maurer, O.; Herter, F.; Bähre, D. The impact of manufacturing parameters on corrosion resistance of additively manufactured AlSi10Mg-samples: A design of experiments approach. *Manuf. Lett.* **2022**, *34*, 29–33. [CrossRef]
9. Hyer, H.; Zhou, L.; Park, S.; Gottsfritz, G.; Benson, G.; Tolentino, B.; McWilliams, B.; Cho, K.; Sohn, Y. Understanding the Laser Powder Bed Fusion of AlSi10Mg Alloy. *Metallogr. Microstruct. Anal.* **2020**, *9*, 484–502. [CrossRef]
10. Ma, H.Y.; Wang, J.C.; Qin, P.; Liu, Y.J.; Chen, L.Y.; Wang, L.Q.; Zhang, L.C. Advances in additively manufactured titanium alloys by powder bed fusion and directed energy deposition: Microstructure, defects, and mechanical behavior. *J. Mater. Sci. Technol.* **2024**, *183*, 32–62. [CrossRef]
11. Maurer, O.; Herter, F.; Bähre, D. Tolerancing the laser powder bed fusion process based on machine capability measures with the aim of process control. *J. Manuf. Process.* **2022**, *80*, 659–665. [CrossRef]
12. Ferro, P.; Meneghello, R.; Razavi, S.M.J.; Berto, F.; Savio, G. Porosity Inducing Process Parameters in Selective Laser MeltedAlSi10Mg Aluminium Alloy. *Phys. Mesomech.* **2020**, *23*, 256–262. [CrossRef]
13. Todaro, C.J.; Easton, M.A.; Qiu, D.; Zhang, D.; Bermingham, M.J.; Lui, E.W.; Brandt, M.; StJohn, D.H.; Qian, M. Grain structure control during metal 3D printing by high-intensity ultrasound. *Nat. Commun.* **2020**, *11*, 142. [CrossRef]
14. Pragana, J.P.M.; Sampaio, R.F.V.; Bragança, I.M.F.; Silva, C.M.A.; Martins, P.A.F. Hybrid metal additive manufacturing: A state–of–the-art review. *Adv. Ind. Manuf. Eng.* **2021**, *2*, 100032. [CrossRef]

15. Rauch, C.; Maurer, O.; Lang, S.-E.; Bähre, D. Serious Games in Academic Education—A Multi-dimensional Sustainability Analysis of Additive Versus Conventional Manufacturing Technologies in a Fictitious Enterprise Project. In *Manufacturing Driving Circular Economy*; Kohl, H., Seliger, G., Dietrich, F., Eds.; Lecture Notes in Mechanical Engineering; Springer International Publishing: Cham, Switzerland, 2023; pp. 819–826. ISBN 978-3-031-28838-8.
16. Mörsdorf, S.; Neumann, D.; Mohnke, J.; Vielhaber, M. Beyond Sustainable Products—Concept for a Positive Impact Product Engineering (PIPE). *Procedia CIRP* **2022**, *105*, 19–24. [CrossRef]
17. Hapuwatte, B.; Seevers, K.D.; Badurdeen, F.; Jawahir, I.S. Total Life Cycle Sustainability Analysis of Additively Manufactured Products. *Procedia CIRP* **2016**, *48*, 376–381. [CrossRef]
18. Kellens, K.; Yasa, E.; Dewulf, W.; Duflou, J.R. Environmental assessment of selective laser melting and selective laser sintering. *Methodology* **2010**, *4*, 5.
19. Dopler, M.; Weiß, C. Energy consumption in metal powder production. *Berg. Huettenmaenn. Monatsh.* **2021**, *166*, 2–8. [CrossRef]
20. Ahmed Obeidi, M.; Mussatto, A.; Groarke, R.; Vijayaraghavan, R.K.; Conway, A.; Rossi Kaschel, F.; McCarthy, E.; Clarkin, O.; O'Connor, R.; Brabazon, D. Comprehensive assessment of spatter material generated during selective laser melting of stainless steel. *Mater. Today Commun.* **2020**, *25*, 101294. [CrossRef]
21. Yang, D.; Fang, H.; Peng, Y.; Fan, J.; Huang, Y.; Wang, K.; Yan, D.; Li, D. Investigation of Spatters in Cold Metal Transfer + Pulse-Based Wire and Arc Additive Manufacturing of High Nitrogen Austenitic Stainless Steel. *J. Mater. Eng. Perform.* **2021**, *30*, 6881–6894. [CrossRef]
22. Noskov, A.; Ervik, T.K.; Tsivilskiy, I.; Gilmutdinov, A.; Thomassen, Y. Characterization of ultrafine particles emitted during laser-based additive manufacturing of metal parts. *Sci. Rep.* **2020**, *10*, 20989. [CrossRef]
23. Sutton, A.T.; Kriewall, C.S.; Leu, M.C.; Newkirk, J.W.; Brown, B. Characterization of laser spatter and condensate generated during the selective laser melting of 304L stainless steel powder. *Addit. Manuf.* **2020**, *31*, 100904. [CrossRef]
24. Harkin, R.; Wu, H.; Nikam, S.; Quinn, J.; McFadden, S. Analysis of Spatter Removal by Sieving during a Powder-Bed Fusion Manufacturing Campaign in Grade 23 Titanium Alloy. *Metals* **2021**, *11*, 399. [CrossRef]
25. Pauzon, C.; Raza, A.; Hanif, I.; Dubiez-Le Goff, S.; Moverare, J.; Hryha, E. Effect of layer thickness on spatter properties during laser powder bed fusion of Ti–6Al–4V. *Powder Metall.* **2023**, *66*, 333–342. [CrossRef]
26. Keaveney, S.; Shmeliov, A.; Nicolosi, V.; Dowling, D.P. Investigation of process by-products during the Selective Laser Melting of Ti6AL4V powder. *Addit. Manuf.* **2020**, *36*, 101514. [CrossRef]
27. Simonelli, M.; Tuck, C.; Aboulkhair, N.T.; Maskery, I.; Ashcroft, I.; Wildman, R.D.; Hague, R. A Study on the Laser Spatter and the Oxidation Reactions During Selective Laser Melting of 316L Stainless Steel, Al-Si10-Mg, and Ti-6Al-4V. *Metall. Mater. Trans. A* **2015**, *46*, 3842–3851. [CrossRef]
28. Murray, J.W.; Speidel, A.; Spierings, A.; Marsh, I.J.; Clare, A.T. Extending powder lifetime in additive manufacturing: Chemical etching of stainless steel spatter. *Addit. Manuf. Lett.* **2022**, *3*, 100057. [CrossRef]
29. Aboulkhair, N.T.; Maskery, I.; Ashcroft, I.; Tuck, C.; Everitt, N.M. The role of powder properties on the processability of Aluminium alloys in selective laser melting. In Proceedings of the Lasers in Manufacturing Conference 2015, Munich, Germany, 22–25 June 2015; p. 6.
30. Weiss, C.; Munk, J.; Haefner, C.L. Investigation Towards AlSi10Mg Powder Recycling Behavior in the LPBF Process and Its Influences on Mechanical Properties. In Proceedings of the 2021 International Solid Freeform Fabrication Symposium, Virtual, 2–4 August 2021; p. 16.
31. Del Re, F.; Contaldi, V.; Astarita, A.; Palumbo, B.; Squillace, A.; Corrado, P.; Di Petta, P. Statistical approach for assessing the effect of powder reuse on the final quality of AlSi10Mg parts produced by laser powder bed fusion additive manufacturing. *Int. J. Adv. Manuf. Technol.* **2018**, *97*, 2231–2240. [CrossRef]
32. Moghimian, P.; Poirié, T.; Habibnejad-Korayem, M.; Zavala, J.A.; Kroeger, J.; Marion, F.; Larouche, F. Metal powders in additive manufacturing: A review on reusability and recyclability of common titanium, nickel and aluminum alloys. *Addit. Manuf.* **2021**, *43*, 102017. [CrossRef]
33. Smolina, I.; Gruber, K.; Pawlak, A.; Ziółkowski, G.; Grochowska, E.; Schob, D.; Kobiela, K.; Roszak, R.; Ziegenhorn, M.; Kurzynowski, T. Influence of the AlSi7Mg0.6 Aluminium Alloy Powder Reuse on the Quality and Mechanical Properties of LPBF Samples. *Materials* **2022**, *15*, 5019. [CrossRef]
34. Sun, X.; Chen, M.; Liu, T.; Zhang, K.; Wei, H.; Zhu, Z.; Liao, W. Characterization, preparation, and reuse of metallic powders for laser powder bed fusion: A review. *Int. J. Extreme Manuf.* **2024**, *6*, 012003. [CrossRef]
35. SLM Solutions Material Data Sheet Al-Alloy AlSi10Mg/EN AC-43000/EN AC-AlSi10Mg 2019.
36. *Norm NF EN ISO 4490:2018*; Metallic Powders—Determination of Flow Rate by Means of a Calibrated Funnel (Hall Flowmeter). International Organization for Standardization: Geneva, Switzerland, 2018.
37. Mittellehner, M.; Danninger, H.; Gierl-Mayer, C.; Gschiel, H. Investigation of the influence of powder moisture on the spreadability using the spreading tester. *Berg. Huettenmaenn. Monatsh.* **2021**, *166*, 14–22. [CrossRef]
38. *EN ISO 3923-1:2018-10*; Metallic Powders—Determination of Apparent Density—Part 1: Funnel Method (ISO 3923-1:2018). German Version EN ISO 3923-1:2018; International Organization for Standardization: Geneva, Switzerland, 2018. [CrossRef]
39. Mahr MahrSurf Surface Texture Parameters. Available online: https://capps.mahr.com/mahr-parameter/html/english/MarSurf/MarSurf.html (accessed on 30 July 2023).

40. Lam, L.P.; Zhang, D.Q.; Liu, Z.H.; Chua, C.K. Phase analysis and microstructure characterisation of AlSi10Mg parts produced by Selective Laser Melting. *Virtual Phys. Prototyp.* **2015**, *10*, 207–215. [CrossRef]
41. Ghio, E.; Cerri, E. Additive Manufacturing of AlSi10Mg and Ti6Al4V Lightweight Alloys via Laser Powder Bed Fusion: A Review of Heat Treatments Effects. *Materials* **2022**, *15*, 2047. [CrossRef] [PubMed]
42. Sert, E.; Schuch, E.; Öchsner, A.; Hitzler, L.; Werner, E.; Merkel, M. Tensile strength performance with determination of the Poisson's ratio of additively manufactured AlSi10Mg samples. *Mater. Werkst.* **2019**, *50*, 539–545. [CrossRef]
43. Friedrich, H.E. (Ed.) *Magnesium Technology: Metallurgy, Design Data, Applications*; Springer: Berlin/Heidelberg, Germany, 2006; ISBN 978-3-540-20599-9.